μ-Conotoxins Targeting the Human Voltage-Gated Sodium Channel Subtype Na$_V$1.7

Kirsten L. McMahon [1], Hue N. T. Tran [1], Jennifer R. Deuis [1], David J. Craik [1], Irina Vetter [1,2,*] and Christina I. Schroeder [1,3,*,†]

1 Institute for Molecular Bioscience, The University of Queensland, Brisbane, QLD 4072, Australia
2 The School of Pharmacy, The University of Queensland, Woolloongabba, QLD 4102, Australia
3 Center for Cancer Research, National Cancer Institute, National Institutes of Health, Frederick, MD 21702, USA
* Correspondence: i.vetter@imb.uq.edu.au (I.V.); c.schroeder@imb.uq.edu.au (C.I.S.)
† Current address: Department of Peptide Therapeutics, Genentech, 1 DNA Way, South San Francisco, CA 94080, USA.

Abstract: μ-Conotoxins are small, potent, peptide voltage-gated sodium (Na$_V$) channel inhibitors characterised by a conserved cysteine framework. Despite promising in vivo studies indicating analgesic potential of these compounds, selectivity towards the therapeutically relevant subtype Na$_V$1.7 has so far been limited. We recently identified a novel μ-conotoxin, SxIIIC, which potently inhibits human Na$_V$1.7 (hNa$_V$1.7). SxIIIC has high sequence homology with other μ-conotoxins, including SmIIIA and KIIIA, yet shows different Na$_V$ channel selectivity for mammalian subtypes. Here, we evaluated and compared the inhibitory potency of μ-conotoxins SxIIIC, SmIIIA and KIIIA at hNa$_V$ channels by whole-cell patch-clamp electrophysiology and discovered that these three closely related μ-conotoxins display unique selectivity profiles with significant variations in inhibitory potency at hNa$_V$1.7. Analysis of other μ-conotoxins at hNa$_V$1.7 shows that only a limited number are capable of inhibition at this subtype and that differences between the number of residues in loop 3 appear to influence the ability of μ-conotoxins to inhibit hNa$_V$1.7. Through mutagenesis studies, we confirmed that charged residues in this region also affect the selectivity for hNa$_V$1.4. Comparison of μ-conotoxin NMR solution structures identified differences that may contribute to the variance in hNa$_V$1.7 inhibition and validated the role of the loop 1 extension in SxIIIC for improving potency at hNa$_V$1.7, when compared to KIIIA. This work could assist in designing μ-conotoxin derivatives specific for hNa$_V$1.7.

Keywords: μ-conotoxins; voltage-gated sodium channels; structure-activity relationships; disulfide-rich peptides; Cys frameworks

Key Contribution: K.L.M., I.V. and C.I.S. conceptualized the project, K.L.M. carried out peptide synthesis, N.M.R.; and electrophysiology with assistance from H.N.T. (peptide chemistry), and J.R.D., and I.V. (electrophysiology). K.L.M. wrote the manuscript which was edited and reviewed by I.V. and C.I.S. All authors read and approved the manuscript prior to submission.

1. Introduction

Marine cone snail venom comprises a diverse mixture of disulfide-rich ion channel modulators called conotoxins [1]. μ-Conotoxins, characterised by a conserved cysteine framework (i.e., CC–C–C–CC), potently inhibit voltage-gated sodium (Na$_V$) channels through a pore blockage mechanism [2]. Although humans express nine different Na$_V$ channel subtypes, μ-conotoxins have a preference for TTX-sensitive (TTX-s) subtypes, Na$_V$1.1–1.4, 1.6 and Na$_V$1.7, over TTX-resistant (TTX-r) subtypes Na$_V$1.5, 1.8 and 1.9 [3–5]. Of particular interest is their inhibitory potency at Na$_V$1.7, as this subtype has therapeutic potential for the treatment of pain [6,7]. However, the translation from hit to drug lead

is hindered by the lack of specificity of μ-conotoxins for Na$_V$ channel subtypes. Given the essential role of Na$_V$ channels in the generation and propagation of action potentials, off-target inhibition of Na$_V$ channels could lead to serious unwanted side-effects. Therefore, identifying μ-conotoxin residues contributing to potent and selective inhibition of human (h)Na$_V$1.7 channels would aid in the development of μ-conotoxin-derived therapeutics for diseases such as chronic pain.

Of the 22 μ-conotoxins characterised to date, only a few display potent inhibition of hNa$_V$1.7 [4,8]. We recently reported the discovery of SxIIIC, a novel μ-conotoxin that inhibits hNa$_V$1.7 with nanomolar potency, though non-selectively [9]. SxIIIC has high sequence homology with two other μ-conotoxins, SmIIIA and CnIIIC [10,11], both of which have been evaluated against mammalian Na$_V$ channels, but only CnIIIC was characterised at human isoforms (hNa$_V$1.7 IC$_{50}$ 485 ± 94 nM) [4]. KIIIA is the only other μ-conotoxin reported to potently inhibit hNa$_V$1.7 (IC$_{50}$ 97–363 nM), although also in a non-selective fashion [8]. Several studies have used KIIIA to investigate residues essential for Na$_V$ inhibition and identified several within the C-terminal α-helix of the peptide [8,12,13]. Those studies resulted in approaches for μ-conotoxin optimisation, including isolating the helical residues and downsizing KIIIA [14–19]. For example, Khoo and colleagues stabilised the KIIIA pharmacophore with a lactam helix, and while the selectivity profile across Na$_V$ channel subtypes remained unaffected, the stabilised helix only yielded micromolar inhibitory potency [14]. In another example, a peptidomimetic based on the KIIIA pharmacophore residues was designed by Brady et al., but only showed micromolar inhibition of Na$_V$1.7 (species not reported) [15]. Other researchers have opted for a combination approach and designed 'mini' and 'midi' variants by combining two μ-conotoxins [16,17], or combining μ-conotoxins and spider toxins [18,19]; however, these too showed limited, non-selective inhibitory potency at hNa$_V$1.7.

In the present study, we used electrophysiology assays to characterise the hNa$_V$ channel selectivity profiles of μ-conotoxins closely related to SxIIIC, including SmIIIA and KIIIA for Na$_V$1.7 (neuronal and pain related) over Na$_V$1.4 (muscle) sodium channel. Through structure-activity relationship analysis of hNa$_V$1.7-inhibiting μ-conotoxins, we discovered point mutations that affect potency and selectivity at hNav1.7. These findings could lead to the development of subtype-selective μ-conotoxin derivatives with potential for therapeutic development.

2. Results

2.1. Oxidation of Native μ-Conotoxins and Analogues

SxIIIC analogues including [Δ1,2]SxIIIC, [R16A]SxIIIC, [R16H]SxIIIC, [R16Q]SxIIIC, [D17A]SxIIIC, [R20A]SxIIIC, [R20E]SxIIIC, [R20H]SxIIIC, [R20Q]SxIIIC, [R20W]SxIIIC were produced using thermodynamic folding as the majority of these peptides produced one major isomer during folding as observed for native SxIIIC, and this major isomer was used for our electrophysiology studies (Figure S2). These peptides were not analysed further using NMR or high-resolution MS (HR-MS) for disulfide bond connectivity confirmation due to the similarities in RP-HPLC chromatogram compared to native SxIIIC suggesting native disulfide connectivity. SmIIIA, the KIIIA analogue [loop1R]KIIIA and SxIIIC analogues ([Δ7,8]SxIIIC, [Δ6–9]SxIIIC and [G8R]SxIIIC) were produced using regioselective folding as they did not form one major isomer during thermodynamic folding conditions (Figure S3). SxIIIC analogues [Δ1,2:R16H]SxIIIC, [Δ1,2:R20A]SxIIIC, [R16H:R20A]SxIIIC and [Δ1,2:R16H:R20A]SxIIIC) produced two main peaks during RP-HPLC analysis following thermodynamic folding (Figure S4) and both peaks were evaluated using 1D ^{1}H NMR (Figure S5) and compared to the NMR spectrum of native SxIIIC. When comparing the NMR spectrum of the SxIIIC peak 1 analogues (blue arrow in Figure S4), several additional or missing peaks were noted in amide region compared to the NMR spectrum of native SxIIIC. The 1D ^{1}H NMR of the second peak more closely resembled native SxIIIC suggesting native disulfide bond conformation (Figure S5), leading us to use the second peak (red arrow in Figure S4) for electrophysiology inhibitory potency evaluation.

2.2. Selectivity of μ-Conotoxins for hNa_V Channel Subtypes

μ-Conotoxin SmIIIA has been reported to only weakly inhibit mammalian $Na_V1.7$ [20,21], despite sharing ~90% sequence homology with the recently described non-selective $hNa_V1.7$ inhibitor SxIIIC [9]. KIIIA has also been shown to inhibit $hNa_V1.7$, albeit at various potencies probably due to the use of different species of $Na_V1.7$ and different recording systems [8,22]. To gain a comprehensive understanding of potency and selectivity of SmIIIA and KIIIA across human Na_V channel subtypes, we assessed the peptides by automated whole-cell patch-clamp electrophysiology in HEK293 cells expressing $hNa_V1.1–1.7/β1$ and CHO cells expressing $hNa_V1.8/β3$ and compared inhibitory potency with our results for SxIIIC in the same cell lines. Concentration-response curves (Figure 1A) were used to determine IC_{50} values for the μ-conotoxins at each channel subtype (Table 1). Comparison of IC_{50} values revealed differences in subtype selectivity between the three μ-conotoxins (Figure 1B). All three μ-conotoxins most potently inhibited $hNa_V1.4$, with SxIIIC (IC_{50} 15 ± 11 nM) and SmIIIA (IC_{50} 14 ± 2 nM) being significantly more potent than KIIIA (IC_{50} 67 ± 15 nM). A similar pattern of inhibitory potency was observed for $hNa_V1.3$ and $hNa_V1.6$, while no differences in potency were seen at $Na_V1.2$. At $Na_V1.1$, SxIIIC and KIIIA showed similar inhibitory potency, while SmIIIA was the least potent. KIIIA, SmIIIA and SxIIIC showed minimal to no inhibition of TTX-r $hNa_V1.5$ and SmIIIA and SxIIIC showed no inhibition of TTX-r $hNa_V1.8$ up to 1 μM (Table 1, Figure S6). Intriguingly, μ-conotoxin inhibitory potency at $hNa_V1.7$ was most varied, with a 9-fold difference between SmIIIA (IC_{50} 41 ± 4 nM) and KIIIA (IC_{50} 379 ± 43 nM) and a 4-fold difference between SmIIIA and SxIIIC (IC_{50} 152 ± 22 nM). This makes SmIIIA, in our hands, the most potent μ-conotoxin inhibitor of $hNa_V1.7$ reported to date.
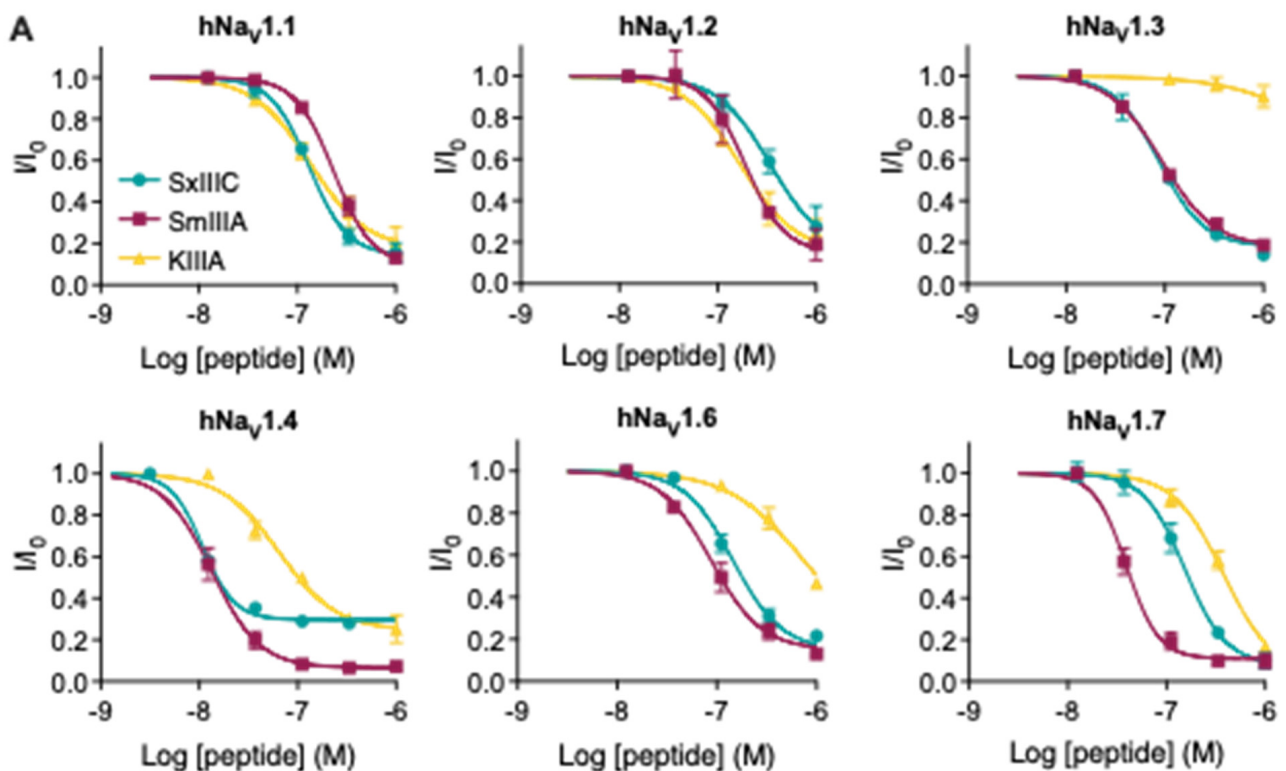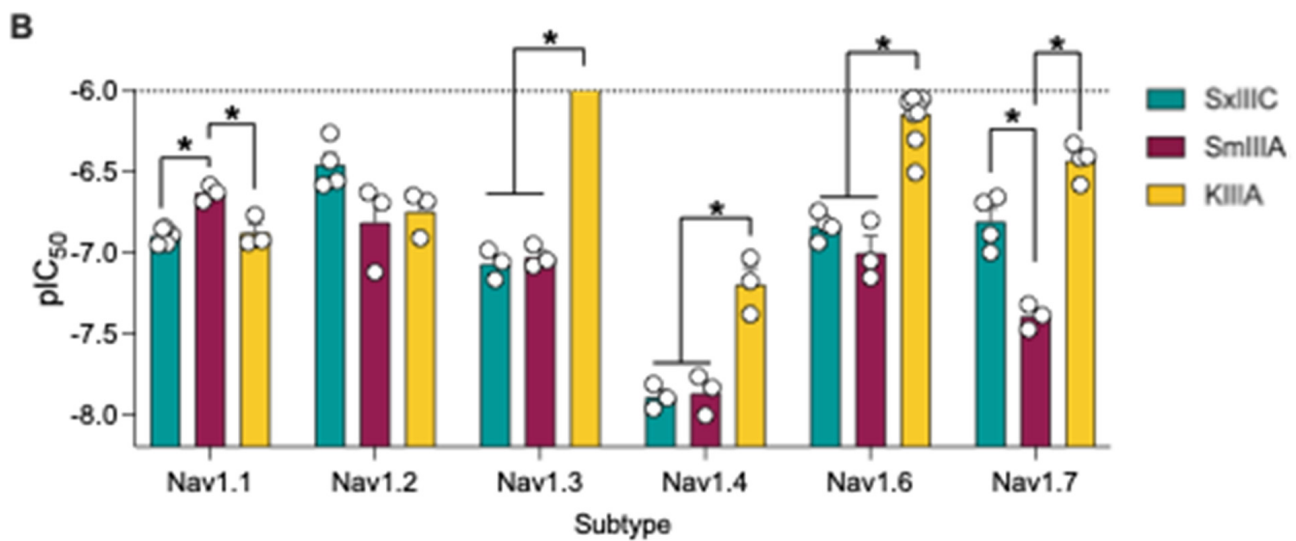

Figure 1. *Cont.*

Figure 1. Comparison of pharmacological inhibitory potency of μ-conotoxins SxIIIC, SmIIIA and KIIIA as assessed by whole-cell patch-clamp electrophysiology across hNa$_V$1.1–1.7/β1 overexpressed in HEK cells. (**A**) Concentration-response curves and (**B**) comparison of μ-conotoxin potency across Na$_V$ channel subtypes. SxIIIC data from [9]. Data are presented as mean ± SEM with individual data points (*n* = 3–10). Statistical significance was calculated by ordinary one-way ANOVA analysis and Tukey's multiple comparisons test (* *p*-value < 0.05).

Table 1. Summary of μ-conotoxin IC$_{50}$ values. IC$_{50}$ values displayed in nM ± SEM.

Subtype	SxIIIC [a]	SmIIIA	KIIIA
Na$_V$1.1	132 ± 12	235 ± 15.0	136 ± 18
Na$_V$1.2	364 ± 54	172 ± 49	186 ± 32
Na$_V$1.3	89 ± 11	95 ± 9	>1000
Na$_V$1.4	15 ± 11	14 ± 2	67 ± 15
Na$_V$1.5	>1000	>1000	>1000
Na$_V$1.6	125 ± 11	106 ± 37	762 ± 77
Na$_V$1.7	152 ± 22	41 ± 4	379 ± 43
Na$_V$1.8	>1000	>1000	>1000

n = 3–10 cells per data point. [a] Results from [9].

2.3. A Limited Number of μ-Conotoxins Display Inhibitory Potency at hNa$_V$1.7

One of the challenges in comparing μ-conotoxin inhibitory potency between different studies is the differences in methods and species (human, mouse, and rat) used. While several μ-conotoxins have been evaluated at hNa$_V$1.7 channels [4,23–25], only a few studies have directly compared μ-conotoxin inhibitory potency at hNa$_V$1.7 in the same cell background. Therefore, we expanded our screen to analyse the hNa$_V$1.7 inhibition of other conotoxins by automated whole-cell patch-clamp electrophysiology. CnIIIC inhibited hNa$_V$1.7 with similar potency to KIIIA (IC$_{50}$ 546 ± 42 nM), whereas TIIIA, GIIIA, GIIIB and SIIIA showed no inhibitory potency at hNa$_V$1.7 up to concentrations of 1 μM (Figure 2). These results are consistent with previous studies where TIIIA and GIIIB (3 μM), assayed using two-electrode voltage-clamp electrophysiology, were inactive at hNa$_V$1.7 [25], and SIIIA (10 μM) only produced ~75% block at hNa$_V$1.7 when evaluated using whole-cell patch-clamp methods [24].
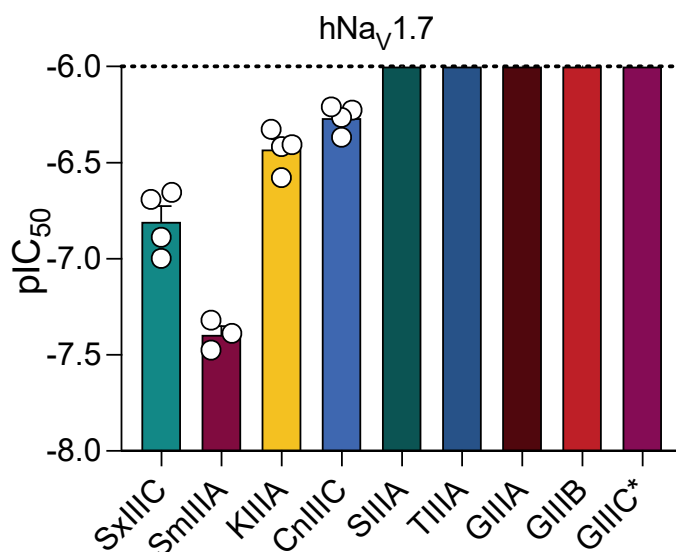
Figure 2. Extended comparison of μ-conotoxins inhibiting hNa$_V$1.7 assessed by whole-cell patch-clamp electrophysiology across hNa$_V$1.7/β1 overexpressed in HEK293 cells. Inhibition of hNa$_V$1.7 by five additional μ-conotoxins, CnIIIC, SIIIA, TIIIA, GIIIA and GIIIB, was evaluated by automated whole-cell patch-clamp methods as described above. CnIIIC was the only additional μ-conotoxin to inhibit hNa$_V$1.7 current. SIIIA, TIIIA, GIIIA and GIIIB displayed no activity up to the highest concentration tested (1 μM). GIIIC was previously found to be inactive at hNa$_V$1.7 at 1 μM [26] * denotes data from references). Data are presented as mean ± SEM with individual data points (*n* = 3–4).

2.4. Charged Residues in Loop 3 Affect Selectivity for hNa$_V$1.7

Interestingly, except for SIIIA, all μ-conotoxins that potently inhibit hNa$_V$1.7 contain five residues within loop 3 (the region between the fourth and fifth cysteine residues), whereas those that were inactive only contained four residues (Table 2). We were therefore interested in investigating the role of the charged residues within this loop in hNa$_V$1.7 inhibition and used SxIIIC as a scaffold to design analogues with either charge-conserving or charge-neutralising substitutions (Table S1). We used SxIIIC in preference over the more active SmIIIA μ-conotoxin due to the ease of synthesis of SxIIIC compared to SmIIIA, which has proved challenging to fold. Whole-cell patch-clamp electrophysiology experiments comparing inhibitory potency of the mutants at Na$_V$1.7 and Na$_V$1.4 (Figure 3) showed that replacement of Arg16 by Ala, [R16A]SxIIIC, resulted in a two-fold loss of inhibition (IC$_{50}$ 334.1 ± 25.5 nM), whereas replacement of Arg16 with a neutral sidechain in [R16Q]SxIIIC did not significantly affect the potency of SxIIIC (Table 3). Interestingly, substituting Arg 16 with His [R16H]SxIIIC (His carries a neutral charge at physiological pH due to its low pKa value, 6.0) we observed a three-fold improvement in inhibition of hNa$_V$1.7 (IC$_{50}$ 66.5 ± 2.5 nM) compared to SxIIIC. We also assessed the neighbouring residue Asp17 and observed no significant change in inhibition with the Ala-replacement analogue [D17A]SxIIIC (IC$_{50}$ 123.5 ± 18.1 nM). Surprisingly, we also observed no difference for the Arg20 analogue [R20A]SxIIIC (IC$_{50}$ 142.3 ± 12.9 nM), despite the analogous residue in KIIIA (Arg 14—KIIIA numbering) having previously been reported to shift subtype selectivity in favour of hNa$_V$1.7 [8].

Table 2. Comparison of μ-conotoxin sequences.

μ-Conotoxin	Sequence	Inhibitory Potency at hNa$_V$1.7
GIIIA	RD**CC**TOOKK**C**KDRQ**C**KOQ-R**CC**A *	No
GIIIB	RD**CC**TOORK**C**KDRR**C**KOM-K**CC**A *	No
GIIIC	RD**CC**TOOKK**C**KDRR**C**KOL-K**CC**A *	No
TIIIA	RHG**CC**KGOKG**C**SSRE**C**ROQ-H**CC** *	No
CnIIIC	G**CC**NGPKG**C**SSKW**C**RDHAR**CC** *	Yes
KIIIA	**CC**N—**C**SSKW**C**RDHSR**CC** *	Yes
SIIIA	ZN**CC**NG—G**C**SSKW**C**RDHAR**CC** *	No
SmIIIA	ZR**CC**NGRRG**C**SSRW**C**RDHSR**CC** *	Yes
SxIIIC	RG**CC**NGRGG**C**SSRW**C**RDHAR**CC** *	Yes

* C-terminal amidation, Z-pyroglutamic acid, O-hydroxyproline.
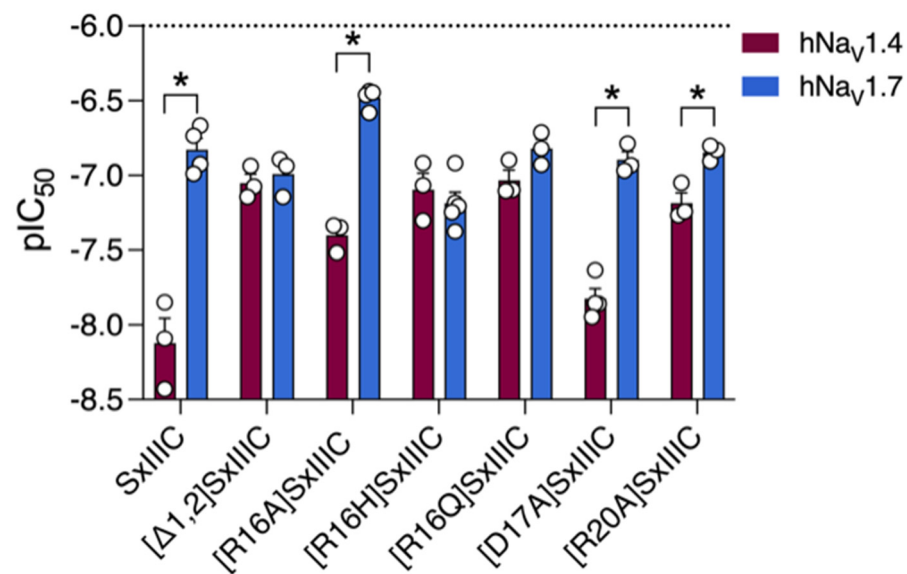
Figure 3. Effect of single SxIIIC mutations on potency and selectivity at hNa$_V$1.7. pIC$_{50}$ values ± SEM are displayed for hNa$_V$1.4 (maroon bars) and hNa$_V$1.7 (blue bars). [R16A]SxIIIC, [D17A]SxIIIC and [R20A]SxIIIC maintained selectivity for hNa$_V$1.4 over hNa$_V$1.7. In contrast, the mutations ([Δ1,2], [R16H], [R16Q]) did not affect inhibitory potency at hNa$_V$1.7 but reduced potency at hNa$_V$1.4, resulting in no significant selectivity between the subtypes. Data are presented as mean ± SEM with individual data points (*n* = 3–5). Statistical significance was determined by unpaired *t*-test (* *p*-value < 0.05).

We next evaluated the inhibitory potency of these analogues, along with truncated SxIIIC, at hNa$_V$1.4 to observe differences in subtype selectivity. Compared to SxIIIC (IC$_{50}$ 12.8 ± 13.0 nM), the R16H and R16Q mutations significantly reduced potency at hNa$_V$1.4 (IC$_{50}$ 80.3 ± 24.7 nM and 99.5 ± 12.9 nM, respectively). Interestingly, this reduction gave IC$_{50}$ values equipotent to hNa$_V$1.7 (Figure 3). The same trend was observed for truncated [~1,2]SxIIIC and the [R20A]SxIIIC analogue, with both displaying reduced potency at hNa$_V$1.4 (IC$_{50}$ 96.3 ± 13.0 nM and 64.8 ± 15.4 nM, respectively) but retaining inhibitory potency at hNa$_V$1.7. Although [R16A]SxIIIC slightly lost potency at hNa$_V$1.4 (IC$_{50}$ 64.8 ± 15.4 nM; Table 3), this did not affect subtype selectivity (Figure 3). In contrast, the D17A mutation in SxIIIC did not affect inhibition of either hNa$_V$1.7 or hNa$_V$1.4 (IC$_{50}$ 14.6 ± 7.7 nM). Together these results reveal that several SxIIIC residues, including Arg1, Gly2, Arg16 and Arg20, may contribute to selectivity between hNa$_V$1.4 and hNa$_V$1.7.

Table 3. Summary of IC_{50} values for SxIIIC analogues at $hNa_V1.7$ and $hNa_V1.4$. IC_{50} displayed in nM $\pm$ SEM.

Analogue	$hNa_V1.7$	Fold Difference to SxIIIC	hNav1.4	Fold Difference to SxIIIC
SxIIIC	152.2 ± 26.8	–	12.8 ± 13.0	–
[Δ1,2]SxIIIC	106.2 ± 19.4	ns	96.3 ± 13.0	↓7-fold
[Δ7,8]SxIIIC	313.6 ± 36.6	↓2-fold	–	–
[Δ6–9]SxIIIC	317.9 ± 100.0	↓2-fold	–	–
[G8R]SxIIIC	155.7 ± 18.9	ns	–	–
[Loop1R]KIIIA	305.1 ± 23.9	↓2-fold *	–	–
[R16A]SxIIIC	334.1 ± 25.5	↓2-fold	38.0 ± 13.0	↓3-fold
[R16H]SxIIIC	66.5 ± 2.5	↑2-fold	80.3 ± 24.7	↓6-fold
[R16Q]SxIIIC	151.3 ± 24.0	ns	99.5 ± 12.9	↓7-fold
[D17A]SxIIIC	123.5 ± 18.1	ns	14.6 ± 7.7	ns
[R20A]SxIIIC	142.3 ± 12.9	ns	64.8 ± 15.4	↓5-fold
[Δ1,2; R16H]	666.6 ± 211.6	↓4-fold	221.4 ± 26.9	↓17-fold
[Δ1,2; R20A]	481.8 ± 646.9	↓3-fold	222.3 ± 70.4	↓17-fold
[R16H; R20A]	888.5 ± 916.4	↓6-fold	247.8 ± 57.7	↓19-fold
[Δ1,2; R16H; R20A]	>1000	–	>1000	–

n = 3–4 cells per data point. ns—no significant difference. * compared to KIIIA. ↓ fold-decrease, and ↑ fold-increase in potency compared to SxIIIC.

2.5. Double and Triple SxIIIC Mutants

Given the minimal disruption to $hNa_V1.7$ potency caused by some SxIIIC mutations, we designed and synthesised double and triple mutant SxIIIC analogues (Table S1). Compared to native SxIIIC, all four analogues lost significant inhibitory potency at both subtypes (Figure 4). At $hNa_V1.7$, the double mutants [Δ1,2; R16H], [Δ1,2; R20A] and [R16H; R20A]SxIIIC lost 4-, 3- and 6-fold potency, respectively (Table 3), whereas at $hNa_V1.4$, the difference was much larger, with all three analogues decreasing potency by an average of 18-fold (Table 3). Notably, the triple mutant [Δ1,2; R16H; R20A] only displayed ~50% inhibition at $hNa_V1.7$ at 1 μM and was not active at $hNa_V1.4$ at 1 μM, the highest concentration tested (Figures 4 and S7).
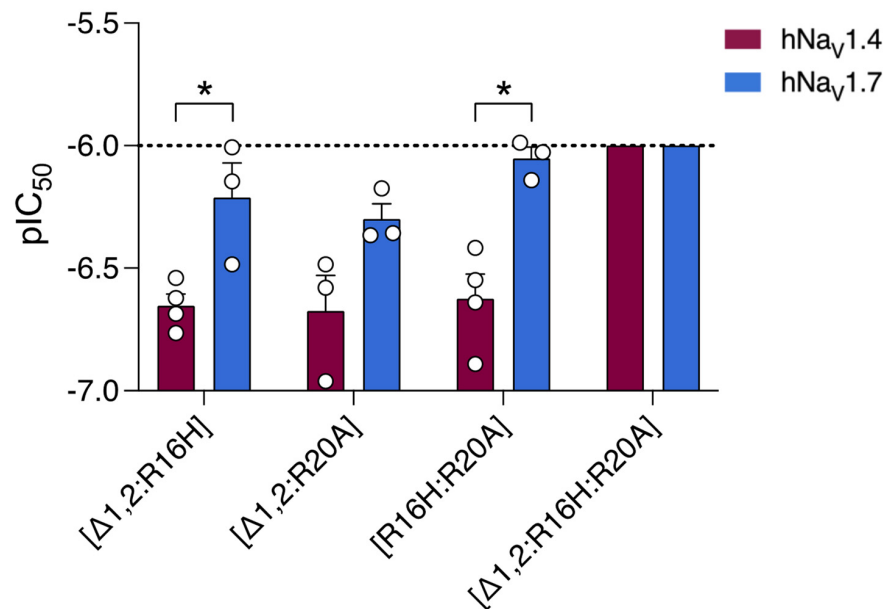
Figure 4. Effect of double and triple SxIIIC mutations on potency and subtype-selectivity at $hNa_V1.4$ and $hNa_V1.7$. Comparative potency of analogues displayed for $hNa_V1.4$ (maroon bars) and $hNa_V1.7$ (blue bars). [Δ1,2; R16H] and [R16H:R20A] maintained selectivity for $hNa_V1.4$ over $hNa_V1.7$. The triple mutant [Δ1,2; R16H; R20A] lost inhibitory potency. Data are presented as mean $\pm$ SEM with individual data points (n = 3–4). Statistical significance was determined by unpaired *t*-test (* *p*-value < 0.05).

## 2.6. Key Structural Differences between hNa$_V$1.7 Inhibiting μ-Conotoxins

The main sequence differences of SxIIIC and SmIIIA compared to KIIIA are, a two-residue N-terminal extension and a four-residue loop 1 extension (Figure 5A). To explore the significance of these extensions, we compared the NMR solution structures (PDB: SxIIIC 6X8R, SmIIIA 1Q2J and KIIIA 2LXG). Notably, while the cysteine framework of 'native' KIIIA [27] differed from SxIIIC and SmIIIA, this does not appear to affect the overall structure of these μ-conotoxins. Comparison of secondary Hα chemical shift deviations from random coil values showed similar shifts between residues Arg13–Ala20 (Figure 5A), indicating conserved structural features across this region. The N-terminal half of the μ-conotoxins displayed the most variation. Backbone alignment of 3D NMR structures between Cys10 and Cys22 (SxIIIC numbering; Figure 5B) showed that the extra residues in loop 1 of SxIIIC and SmIIIA extend the top half of the structure. We propose that this section contributes to the increased potency of these two μ-conotoxins at hNa$_V$1.7. Furthermore, a substitution at Ala19 in SxIIIC to Ser19 in SmIIIA and KIIIA did not appear to affect the shifts for this residue. However, the neighbouring residue Arg20 (SxIIIC numbering) did show differences between the three μ-conotoxins and suggesting a different side-chain orientation of this residue.
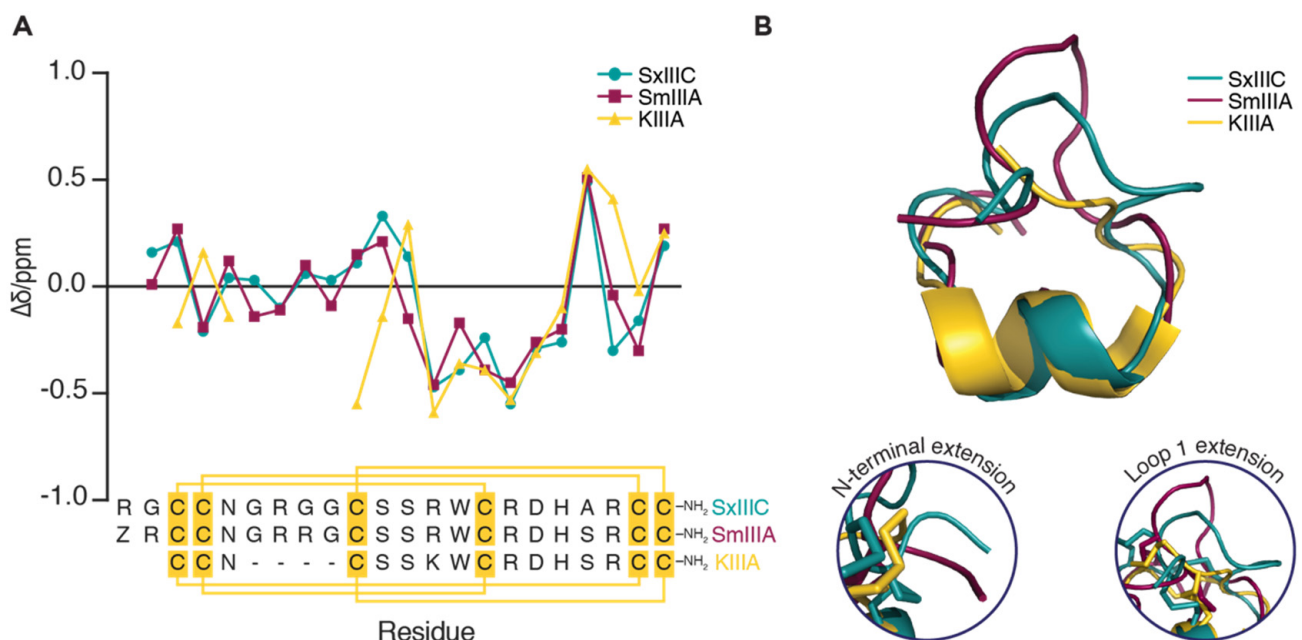
Figure 5. Structural comparison of μ-conotoxins SxIIIC, SmIIIA and KIIIA. (A) Comparison of secondary Hα-chemical shifts compared to random coil values [28] for three μ-conotoxins SxIIIC, SmIIIA and KIIIA [29]. Sequence alignment shows high sequence homology between μ-conotoxins with disulfide connectivity (yellow lines). **(B)** Representative 3D NMR structures (PDB: SxIIIC 6X8R, SmIIIA 1Q2J and KIIIA 2LXG) of μ-conotoxins superimposed across residues Cys10–Cys22 (SxIIIC numbering; RMSD = 1.146 Å) shows how the conserved C-terminal residues contribute to similar backbone fold, whereas the N-terminal and loop 1 extensions (inserts) extend the structures of SxIIIC and SmIIIA.

2.7. N-Terminal Deletion Does Not Significantly Affect the Potency of SxIIIC

To assess the effects of N-terminal extensions observed in SxIIIC and SmIIIA compared to KIIIA, we designed the truncated SxIIIC analogue [Δ1,2]SxIIIC (Table S1). Due to difficulties synthesising native and modified SmIIIA, only SxIIIC and KIIIA analogues were pursued. In whole-cell patch-clamp electrophysiology experiments, we found that deletion of the N-terminal residues of SxIIIC did not significantly affect potency at hNa$_V$1.7 (IC$_{50}$ 106.2 ± 19.4 nM) compared to native SxIIIC (IC$_{50}$ 152.2 ± 26.8 nM) ($p > 0.05$) (Figure 6).
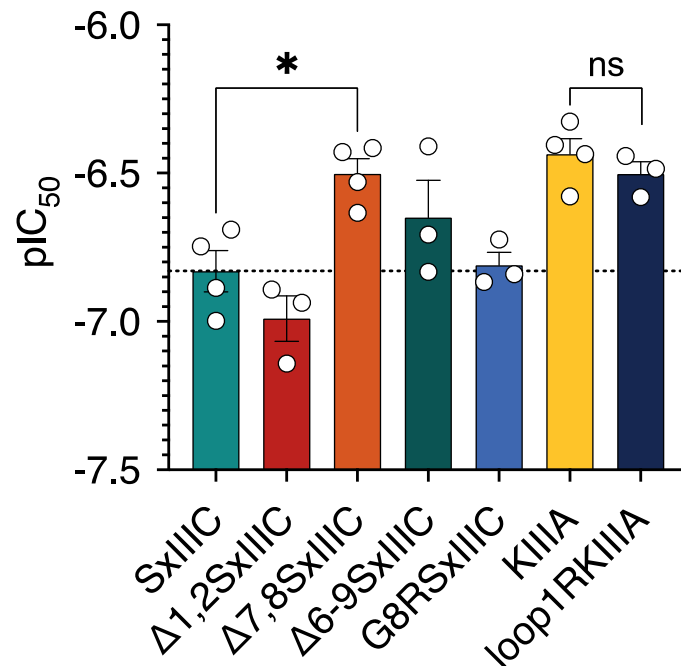
Figure 6. Effects of N-terminal and loop 1 mutations on μ-conotoxin potency at hNa$_V$1.7. Comparative potency of analogues at hNa$_V$1.7. N-terminal deletions of SxIIIC ([Δ1,2]SxIIIC) and the addition of loop 1 residues ([loop1R]KIIIA) into KIIIA did not significantly affect potency compared to native μ-conotoxins. Loop 1 deletions of SxIIIC ([Δ7,8] significantly reduced potency of SxIIIC, similar to that of KIIIA. Introduction of an additional charged residue into SxIIIC loop 1 ([G8R]SxIIIC) did not alter potency compared to native SxIIIC. Data are presented as mean ± SEM with individual data points (*n* = 3–4). Statistical significance for SxIIIC analogues was determined by ordinary one-way ANOVA with Dunnett's multiple comparisons test compared to native SxIIIC (* *p*-value < 0.05). Statistical significance for KIIIA and loop1 RKIIIA was determined by unpaired *t*-test (* *p*-value < 0.05).

2.8. Loop 1 Truncation Reduces Potency of SxIIIC at hNa$_V$1.7

Interestingly, when we deleted residues within loop 1 of SxIIIC ([Δ7,8]SxIIIC), we observed reduced potency (IC$_{50}$ 313.6 ± 36.6 nM; Table 3) compared to native SxIIIC. As these IC$_{50}$ values were similar to KIIIA (IC$_{50}$ 383.5 ± 15.2 nM; Figure 6), which has a similarly truncated loop 1, these results suggest that the additional loop 1 residues in SxIIIC are required for increased inhibition of hNa$_V$1.7 compared to KIIIA. Furthermore, when we introduced an extra charged residue into loop 1 of SxIIIC ([G8R]SxIIIC) to mimic SmIIIA, we did not observe a significant change in potency (IC$_{50}$ 155.7 ± 18.9 nM; Table 3) compared to SxIIIC. This observation suggests that the additional charged residue in loop 1 of SmIIIA does not cause the 4.4-fold difference in inhibition of hNa$_V$1.7 observed between SxIIIC and SmIIIA. Unfortunately, previously mentioned difficulties in producing SmIIIA limited our ability to confirm this using SmIIIA analogues. Finally, when modifying KIIIA to include additional residues within loop 1 ([loop1R]KIIIA), we expected this analogue to mimic the inhibitory potency of SxIIIC. However, we observed no significant change in potency (IC$_{50}$ 305.1 ± 23.9 nM; Table 3) compared to native KIIIA, suggesting that either the disulfide connectivity of KIIIA is unfavourable for loop 1 extensions, or that this peptide binds in a different orientation.

3. Discussion

μ-Conotoxins are potent inhibitors of disease-relevant Na$_V$ channels, yet their promiscuous activity across different subtypes has hindered their potential for therapeutic development, as off-target activity may lead to undesirable side effects. Due to an apparent lack of inhibitory potency of many μ-conotoxins at hNa$_V$1.7, only a few studies have anal-

ysed structure–activity relationships at this subtype. Here, we identified key features of μ-conotoxins of SxIIIC, SmIIIA and KIIIA that contribute to inhibition of hNa$_V$1.7, including loop length, and single point mutations that affect selectivity towards hNa$_V$1.4 without affecting potency at hNa$_V$1.7.

We initially assessed two μ-conotoxins, SmIIIA and KIIIA, by whole-cell patch-clamp methods, to evaluate their selectivity profiles for hNa$_V$ channel subtypes. Compared to SxIIIC [9], these highly homologous μ-conotoxins displayed distinct selectivity profiles (Table 4). Interestingly, our results are not in agreement with mammalian selectivity profiles reported previously for SmIIIA [20] or KIIIA [12,30]. While these inconsistencies may be attributed to the use of different techniques (two-electrode voltage- or patch-clamp methods on oocytes vs. mammalian cells; manual vs. automated techniques), or the presence of different auxiliary β-subunits, the most plausible explanation is species differences (human, rat or mouse). The earlier studies used rat isoforms, as opposed to the human subtypes used in this study. Despite the high sequence homology between species, it is not uncommon for μ-conotoxins to display different inhibitory potency across species. Such interspecies variability highlights the need to study human isoforms when evaluating the therapeutic potential of μ-conotoxins. We showed that SmIIIA inhibits hNa$_V$1.7 more potently than both SxIIIC (~4-fold) and KIIIA (~10-fold). In our hands, SmIIIA is the most potent μ-conotoxin inhibitor of hNa$_V$1.7 (IC$_{50}$ 41 $\pm$ 4 nM) reported to date.

Table 4. Comparison of μ-conotoxin selectivity profiles of hNa$_V$ channels.

μ-Conotoxin	Selectivity Profile
SxIIIC	1.4 > 1.3 > 1.6 ≈ 1.1 ≈ **1.7** > 1.2 >> 1.5 ≈ 1.8
SmIIIA	1.4 > **1.7** > 1.3 ≈ 1.6 > 1.2 > 1.1 >> 1.5 ≈ 1.8
KIIIA	1.4 > 1.1 > 1.2 > **1.7** > 1.6 > 1.3 >> 1.5 ≈ 1.8

As only a limited number of μ-conotoxins have been assessed at human Na$_V$ isoforms, we explored the ability of μ-conotoxins GIIIA, GIIIB, TIIIA, CnIIIC and SIIIA to inhibit hNa$_V$1.7 by whole-cell patch-clamp methods. CnIIIC was found to be equipotent with KIIIA, whereas a lack of inhibitory potency was observed for the other four μ-conotoxins at the highest concentration tested (1 μM). The results for GIIIA, GIIIB and TIIIA were consistent with the homologous μ-conotoxin GIIIC, previously shown to be inactive at hNa$_V$1.7 [23]. While the results of SIIIA were expected [24], it is interesting that SIIIA (at 10 nmol, corresponding to 0.7 mg/kg) can produce an analgesic effect in a murine model of inflammatory pain [31]. Leipold et al. [3] introduced the Domain II pore loop of hNa$_V$1.7 into rNa$_V$1.4 and identified Asn889 (hNa$_V$1.7) as responsible for the reduced sensitivity of hNa$_V$1.7 to SIIIA. The corresponding residue in mNa$_V$1.7 is conserved, suggesting that this residue alone may not be responsible for species differences. Another possible explanation for the lack of activity of SIIIA at hNa$_V$1.7 may be the apparent low net charge (+1.7) compared to hNa$_V$1.7 inhibiting μ-conotoxins, which all have a net charge of +2.8 to +4.7 (Figure 7). While μ-conotoxins share key similarities such as a conserved disulfide network, the backbone sequences between these cysteines, referred to as loops 1–3, are varied. For example, GIIIA, GIIIB, GIIIC, PIIIA and TIIIA all have four residues in loop 3 (between Cys4–Cys6) and are classed in the M4-branch μ-conotoxins [32]. In contrast, SIIIA, KIIIA, CnIIIC, SmIIIA and SxIIIC have five residues in loop 3 and are classified as M5-branch μ-conotoxins [32]. M4-branch μ-conotoxins have an increased overall net charge (≥+4.8) compared to M5-branch μ-conotoxins (Figure 7), suggesting that overall net change may contribute to μ-conotoxins' ability to inhibit hNa$_V$1.7.
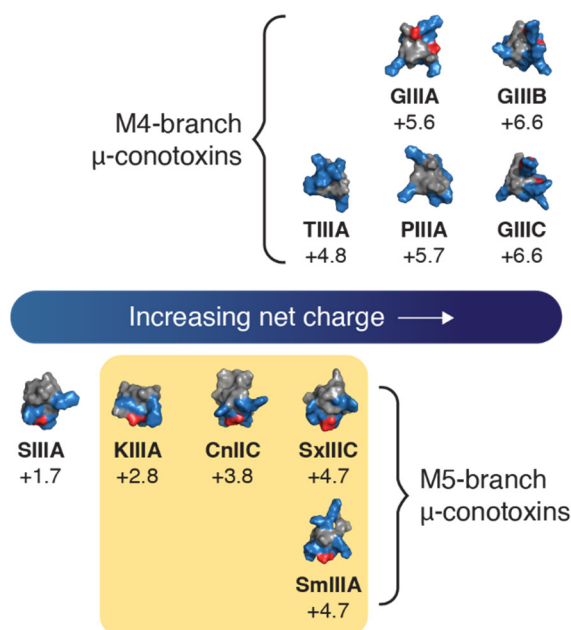
Figure 7. Representation of the surface profile of μ-conotoxins and corresponding net charge.
Colours represent charged residues (basic–blue; acidic–red; neutral–grey). μ-Conotoxins active
against hNa$_V$1.7 (yellow shaded box) appear on the M5-branch and have an overall net charge of
between +2.8–4.7.

To explore the role of residues in loop 3, we designed a series of μ-conotoxin analogues,
opting to base our designs on SxIIIC, as opposed to the more potent SmIIIA, due to
difficulties in folding the latter μ-conotoxin. Our experience in synthesising SmIIIA is
consistent with literature that reports synthetic production of SmIIIA often yields multiple
isomers when folded under thermodynamic conditions [33]. In the current study we used
a regioselective approach for SmIIIA synthesis to ensure desired disulfide connectivity;
however, despite successful direction of the disulfide bonds during regioselective SmIIIA
synthesis, the yield was low, and purification proved surprisingly challenging considering
the high sequence homology with SxIIIC. In contrast, SxIIIC could easily be oxidised
thermodynamically, resulting in a single major isomer, or using regioselective oxidation. In
addition to targeted Ala-mutations in SxIIIC, in lieu of an Ala-walk (replacing all non-Cys
and Gly residues with Ala), which has been conducted for other μ-conotoxins [12,25,34,35],
we were interested in exploring the consequences of different chemical properties at specific
residues and thus employed rational design for our SxIIIC analogues.

Replacement of Arg16 of SxIIIC with an Ala ([R16A]SxIIIC) reduced potency two-fold
at hNa$_V$1.7. Our results are in contrast to those of McArthur and colleagues, who found
Ala-replacement of the equivalent residue in KIIIA ([R10A]KIIIA) increased inhibition at
hNa$_V$1.7 [8]. That study did not report the disulfide connectivity of KIIIA, and activity
studies lacked β-subunit expression, which has since been shown to affect the affinity
of μ-conotoxins to Na$_V$ channels [21]. Interestingly, we observed improved potency at
hNa$_V$1.7 and decreased inhibition at hNa$_V$1.4 with a SxIIIC His-substitution at position
16, [R16H]SxIIIC. Whilst His theoretically carries a neutral charge at physiological pH, the
charge state of this amino acid can be highly dependent on the environment created by sur-
rounding amino acids and may carry a positive charge, which together with the additional
bulk of the amino acid compared to the native Arg could explain the improved potency at
Na$_V$1.7. Another analogue, [R20A]SxIIIC, also did not affect hNa$_V$1.7 inhibition and lost
potency at hNa$_V$1.4; however, the peptide did not display altered subtype selectivity. These
results are also in contrast to Arg20 KIIIA mutations previously reported [8] that shifted
selectivity towards hNa$_V$1.7 from rNa$_V$1.2 and rNa$_V$1.4.

Using the three SxIIIC analogues that did not affect inhibition at hNa$_V$1.7 but reduced potency at hNa$_V$1.4, we designed and synthesised a series of double and triple mutants. None of the multiple SxIIIC mutant analogues improved potency at either channel tested (hNa$_V$1.4 and hNa$_V$1.7) or shifted selectivity in favour of hNa$_V$1.7. While these results were disappointing, they were not completely unexpected. μ-Conotoxins have naturally evolved to potently and selectively target Na$_V$ channels, and the manipulation of such an evolutionarily refined natural product can be challenging. However, one explanation for the loss in potency may have been in choosing the incorrect isomer following thermodynamic oxidation (Figures S4 and S5). To assess if the folding contributed to the loss in inhibitory potency, we additionally tested the first eluting peak for each of the analogues against hNa$_V$1.4 and found them to be less active than the second eluting peak (Figure S7). In summary, none of the multiple mutant analogues improved the potency or selectivity of SxIIIC.

Given the potential clinical applications of selective Na$_V$1.7 inhibition, we compared the NMR structures of three μ-conotoxins with potent inhibition of hNa$_V$1.7, i.e., SxIIIC, SmIIIA and KIIIA. We identified two major differences, in the form of extensions in the N-terminal and loop 1 residues of SxIIIC and SmIIIA, both absent in KIIIA. As many residues within the highly conserved C-terminal region of the μ-conotoxins have been shown to be critical for μ-conotoxin inhibition [8,12,13,36], we proposed that these structural differences observed in the N-terminal region influenced the differences in the inhibitory potency at hNa$_V$1.7. To evaluate this, we designed an additional series of μ-conotoxins analogues using SxIIIC.

By creating a truncated N-terminal analogue, we found that the N-terminal residues of SxIIIC are not essential for inhibition of hNa$_V$1.7. However, truncated SxIIIC, which maintained inhibitory potency at hNa$_V$1.7, compared to native SxIIIC, displayed decreased potency at hNa$_V$1.4. The N-terminal extension of SxIIIC, and potentially SmIIIA, is likely to be essential for inhibition at other subtypes, as seen with μ-conotoxin KIIIB (identical to KIIIA but with a two-residue N-terminal extension) which inhibits rNa$_V$1.2 with 5-fold greater affinity than KIIIA [27]. These results are consistent with truncated SIIIA, which showed that these N-terminal residues played a non-essential role in rNa$_V$1.2 inhibition [34]. It could be suggested that these N-terminal residues play a role in guiding the μ-conotoxin to the binding site in different Na$_V$ channel subtypes. In contrast to the N-terminal extension, we discovered that residues within loop 1 of SxIIIC influenced inhibition of hNa$_V$1.7. When loop 1 residues were removed to mimic KIIIA, the potency of SxIIIC reverted to IC$_{50}$ values similar to KIIIA. As many studies interested in optimising KIIIA for Na$_V$1.7 inhibition have focused on downsizing or reducing the μ-conotoxins to only retain residues contributing to the pharmacophore [14–16], our findings identify for the first time the importance of the residues within loop 1 of SxIIIC for potent inhibition of hNa$_V$1.7. Interestingly, when we reintroduced extra loop 1 residues into KIIIA, we did not observe the expected improved potency. By revisiting the NMR structure, we observed that although KIIIA had a different disulfide connectivity to SxIIIC, the overall conformation of the disulfide bonds did not change. This suggests that KIIIA with I–V, II–IV, III–VI connectivity might not be optimal for the addition of residues in loop 1 and this could be explored in future studies.

In addition to improved selectivity for Na$_V$1.7, which is essential to avoid severe systemic side effects, species selectivity of the μ-conotoxins currently limits preclinical efficacy test in relevant rodent models of pain. Accordingly, future work, such as modelling or structural studies using relevant channel states and subtypes, will be required to facilitate drug development efforts, although oral delivery of peptides remains a challenge that would likely limit μ-conotoxin-based therapeutics to parenteral administration.

In conclusion, we have identified that the number of residues within loops 1 and 3 of SxIIIC, SmIIIA and KIIIA contributes to potency at hNa$_V$1.7. Overall, the findings of this study provide valuable information for future design of hNa$_V$1.7 specific μ-conotoxin derived inhibitors.

4. Methods

4.1. Peptide Synthesis

KIIIA, SIIIA, SxIIIC and analogues including [Δ1,2]SxIIIC, [R16A]SxIIIC, [R16H]SxIIIC, [R16Q]SxIIIC, [D17A]SxIIIC, [R20A]SxIIIC, [R20E]SxIIIC, [R20H]SxIIIC, [R20Q]SxIIIC, [R20W]SxIIIC, [Δ1,2:R16H]SxIIIC [Δ1,2:R20A]SxIIIC, [R16H:R20A]SxIIIC and [Δ1,2:R16H:R20A]SxIIIC) were synthesised using methods described earlier [9]. Protecting groups trityl (Trt), acetamidomethyl (Acm) and 4,4′-dimethylsulfinylbenzhydryl (Msbh) were used for regioselective protection of SmIIIA and SxIIIC analogues ([Δ7,8]SxIIIC, [Δ6–9]SxIIIC and [G8R]SxIIIC) with connectivity Cys3–Cys15(Msbh)/Cys4–Cys21(Acm) / Cys10–Cys22(Trt). The KIIIA analogue [loop1R]KIIIA was produced with connectivity Cys1–Cys15(Msbh)/Cys2–Cys9(Acm)/Cys4–Cys16(Trt). All peptides were assembled on a CEM Liberty Prime automatic synthesiser (CEM, Matthews, NC, USA) using rink amide-AM resin. Peptides were cleaved from solid support and side chains simultaneously deprotected in 92.5% trifluoroacetic acid (TFA)/2.5% triisopropylsilane/2.5% water/2.5% 2,2-(ethylenedioxy)diethanethiol for 2 h at room temperature. Excess TFA acid was evaporated by N_2 flow, followed by peptide precipitation in ice-cold diethyl ether and centrifugation. Peptides were redissolved in solvent B (50% acetonitrile (ACN)/0.01% TFA) and lyophilised. TIIIA, GIIIA and GIIIB were synthesised as previously described [25,34]. A list of peptide sequences can be found in Supplementary Materials (Table S1).

4.2. Oxidation

Most SxIIIC analogues were oxidised thermodynamically to form disulfide bonds as described earlier [9]. However, due to difficulties obtaining the desired connectivity using thermodynamic oxidation, some peptides were oxidised using orthogonal protection of pairs of Cys residues. This regioselective oxidation was done as described previously [26,37], whereby linear peptides with Trt group removed were dissolved in acetic acid (2 mg/mL) and stirred at room temperature. To oxidise the first Cys pair, one equivalent of I_2 (dissolved in MeOH) was added dropwise until the reaction turned pale-yellow and the colour persisted. Five equivalents of free Trp were added to minimise side-reactions with iodine. Following 15 min of stirring, the reaction was diluted with water and hydrochloric acid to a final volume of 50% acetic acid and 1% hydrochloric acid. To remove the Acm group and form the second disulfide bond, eight equivalents of I_2 were added to the reaction and stirred for a further 30 min. The reaction was quenched with aqueous ascorbic acid until the solution became colourless. The intermediate product was isolated by RP-HPLC on a Shimadzu LC-20AT system equipped with an SPD-20A Prominence UV/VIS detector, and a FRC-10A fraction collector. Peptides were diluted to <2% acetic acid and loaded onto a Gemini, 5 μm C18 110 Å, 250 × 10 mm column (Phenomenex, Torrance, CA, USA). Peptides were purified using linear gradient between 5–25% solvent B over 40 min at 3 mL/min (solvent A: 0.05% TFA in H_2O; solvent B: 90% ACN/0.05% TFA in H_2O). Fractions containing the desired product were identified by electrospray ionisation-mass spectrometry (ESI-MS) and lyophilised. To remove the Msbh protecting groups and form the final disulfide bond, peptides were dissolved in TFA (1 mg/mL) and cooled on ice. Five equivalents of free Trp, dimethyl sulfate (1% *v/v*) and 20 equivalents of NaI were added and stirred for 15 min. The reaction was quenched by diluting the reaction with aqueous ascorbic acid (10 nM; 15 times the initial volume of TFA). The final product was isolated by RP-HPLC using a Gemini, 5 μm C18 110 Å, 250 × 5 mm column and a linear gradient 0–20% solvent B at 1 mL/min over 40 min. Fractions containing the desired product were identified by ESI-MS (Shimadzu LCMS-2020), lyophilised and stored at −20 °C. For analytical RP-HPLC and ESI-MS of the final products, see Figures S1–S4.

4.3. Cell Culture

HEK293 cells heterologously expressing hNa$_V$1.1–1.7/β1 (SB Drug Discovery, Glasgow, UK) or CHO cells heterologously expressing hNa$_V$1.8/β3 in a tetracycline-inducible system (ChanTest, Cleveland, OH, USA) were maintained in Minimum Essential Medium

Eagle (M5650) supplemented with 10% *v/v* foetal bovine serum, 2 mM L-glutamine, and the selection antibiotics as recommended by the manufacturer. Cells were incubated at 37 °C with 5% CO_2 and split every 3–4 days when reaching 70–80% confluency using the dissociation reagent TrypLE Express (Thermo Fisher Scientific, Scoresby, VIC, Australia). Expression of $hNa_V1.8$ was induced by the addition of tetracycline (1 µg/mL) for 48 h prior to assays.

4.4. Whole-Cell Patch-Clamp Electrophysiology Assays

Automated whole-cell patch-clamp recordings were performed with a QPatch-16 automated electrophysiology platform (Sophion Bioscience, Ballerup, Denmark) as previously described [9].

The extracellular solution consisted of (in mM) 145 NaCl, 4 KCl, 2 $CaCl_2$, 1 $MgCl_2$, 10 HEPES, and 10 glucose, pH to 7.4 with NaOH (adjusted to 305 mOsm/L with sucrose). The intracellular solution consisted of (in mM) 140 CsF, 1 EGTA, 5 CsOH, 10 HEPES, and 10 NaCl, pH to 7.3 with CsOH (adjusted to 320 mOsm/L with sucrose). Peptides were diluted in extracellular solution with 0.1% bovine serum albumin and each concentration was incubated for 5 min. $hNa_V1.1$–1.7 currents were elicited by a 50 ms test pulse to −20 mV from a holding potential of −90 mV (repetition interval 20 s). $hNa_V1.8$ currents were elicited by a 50 ms test pulse to +10 mV from a holding potential of −90 mV (repetition interval 20 s) in the presence of TTX (1 µM) to inhibit endogenous TTX-sensitive current in CHO cells. Recordings were taken at ambient room temperature (22 °C). Peak current post-peptide addition (I) was normalised to peak current of buffer control (I_0). IC_{50}s were determined by plotting difference in peak current (I/I_0) and log peptide concentration. Concentration-response curves were fitted using the log (inhibitor) vs. response-variable slope (four parameters) Equation (1) to obtain pIC_{50} values for each biological replicate.

$$y = 1/(1 + 10^{((LogIC_{50} − x) × HillSlope))} \tag{1}$$

The corresponding IC_{50}s were used to compute mean ± standard error of the mean from at least *n* = 3 biological replicates.

5. Data Analysis

Data were analysed using GraphPad Prism 9.3.1. Statistical significance, defined as $p < 0.05$, was determined using One-way ANOVA with Tukey's multiple comparison of IC_{50} or pIC_{50} values fitted for individual biological replicates as described above.

Supplementary Materials: The following supporting information can be downloaded at: https: //www.mdpi.com/article/10.3390/toxins14090600/s1. Figure S1: Analytical RP-HPLC traces with corresponding ESI-MS spectra of native µ-conotoxins used in this study; Figure S2: Analytical RP-HPLC traces with corresponding ESI-MS spectra of single mutants and N-terminus truncated SxIIIC analogues used in this study; Figure S3: Crude and analytical RP-HPLC traces with corresponding ESI-MS spectra following regioselective oxidation of SxIIIC analogues used in this study; Figure S4: RP-HPLC traces repre-senting the crude oxidation of double and triple mutant SxIIIC analogues highlighting the two main folding isomers (peak 1—blue arrow, and peak 2—red arrow), and analytical RPHPLC traces of isolated fractions (peak 2—red arrow), with corresponding ESI-MS spectra of peak 2 (red arrow); Figure S5: 1D 1H NMR spectra of the amide region of the first and second peaks from the double and triple mutant SxIIIC analogues; Figure S6: Concentration response curves of A KIIIA, SmIIIA, SxIIIC at TTX-r hNaV1.5/b1 overexpressed in HEK293 cells, and B SmIIIA and SxIIIC at TTX-r hNaV1.8/b3 overexpressed in CHO cells using automated whole cell patch clamp electrophysiol-ogy; Figure S7: Concentration response curves for the two major peaks (First peak—A, blue arrow in Figure S4; Second peak—B, red arrow in Figure S4) of the double and triple mutants against hNaV1.4 as assessed by whole-cell patch-clamp electrophysiology; Table S1: Sequence table of µ-conotoxins and analogues used in this study.

References

1. Olivera, B.M.; Seger, J.; Horvath, M.P.; Fedosov, A.E. Prey-Capture Strategies of Fish-Hunting Cone Snails: Behavior, Neurobiology and Evolution. *Brain Behav. Evol.* **2015**, *86*, 58–74. [CrossRef]
2. Hui, K.; Lipkind, G.; Fozzard, H.A.; French, R.J. Electrostatic and Steric Contributions to Block of the Skeletal Muscle Sodium Channel by μ-Conotoxin. *J. Gen. Physiol.* **2002**, *119*, 45–54. [PubMed]
3. Leipold, E.; Markgraf, R.; Miloslavina, A.; Kijas, M.; Schirmeyer, J.; Imhof, D.; Heinermann, S.H. Molecular determinants for the subtype specificity of μ-conotoxin SIIIA targeting neuronal voltage-gated sodium channels. *Neuropharmacology* **2011**, *61*, 105–111. [CrossRef] [PubMed]
4. Markgraf, R.; Leipold, E.; Schirmeyer, J.; Paolini-Bertrand, M.; Hartley, O.; Heinemann, S.H. Mechanism and molecular basis for the sodium channel subtype specificity of μ-conopeptide CnIIIC. *Br. J. Pharmacol.* **2012**, *167*, 576–586. [CrossRef]
5. Li, R.A.; Ennis, I.L.; Xue, T.; Nguyen, H.M.; Tomaselli, G.F.; Godin, A.L.; Marban, E. Molecular Basis of Isoform-specific μ-Conotoxin Block of Cardiac, Skeletal Muscle, and Brain Na+ Channels. *J. Biol. Chem.* **2003**, *278*, 8717–8724. [PubMed]
6. Vetter, I.; Deuis, J.R.; Mueller, A.; Israel, M.R.; Starobova, H.; Zhang, A.; Rash, L.D.; Mobli, M. NaV1.7 as a pain target—From gene to pharmacology. *Pharmacol. Ther.* **2017**, *172*, 73–100. [PubMed]
7. Dib-Hajj, S.D.; Waxman, S.G. Sodium Channels in Human Pain Disorders: Genetics and Pharmacogenomics. *Annu. Rev. Neurosci.* **2019**, *42*, 87–106.
8. McArthur, J.R.; Singh, G.; McMaster, D.; Winkfein, R.; Tieleman, D.P.; French, R.J. Interactions of Key Charged Residues Contributing to Selective Block of Neuronal Sodium Channels by μ-Conotoxin KIIIA. *Mol. Pharmacol.* **2011**, *80*, 573–584. [CrossRef]
9. McMahon, K.L.; Tran, H.N.T.; Deuis, J.R.; Lewis, R.J.; Vetter, I.; Schroeder, C.I. Discovery, Pharmacological Characterisation and NMR Structure of the Novel μ-Conotoxin SxIIIC, a Potent and Irreversible NaV Channel Inhibitor. *Biomedicines* **2020**, *8*, 391. [CrossRef]
10. West, P.J.; Bulaj, G.; Garrett, J.E.; Olivera, B.M.; Yoshikami, D. μ-Conotoxin SmIIIA, a potent inhibitor of tetrodotoxin-resistant sodium channels in amphibian sympathetic and sensory neurons. *Biochemistry* **2002**, *41*, 15388–15393.
11. Favreau, P.; Benoit, E.; Hocking, H.G.; Carlier, L.; D'hoedt, D.; Leipold, E.; Markgraf, R.; Schlumberger, S.; Cordova, M.A.; Gaertner, H.; et al. A novel μ-conopeptide, CnIIIC, exerts potent and preferential inhibition of NaV1.2/1.4 channels and blocks neuronal nicotinic acetylcholine receptors. *Br. J. Pharmacol.* **2012**, *166*, 1654–1668. [CrossRef] [PubMed]
12. Zhang, M.M.; Green, B.R.; Catlin, P.; Fiedler, B.; Azam, L.; Chadwick, A.; Terlau, H.; McArthur, J.R.; French, R.J.; Gulyas, J.; et al. Structure/function characterization of μ-conotoxin KIIIA, an analgesic, nearly irreversible blocker of mammalian neuronal sodium channels. *J. Biol. Chem.* **2007**, *282*, 30699–30706. [PubMed]

13. Van der Haegen, A.; Peigneur, S.; Tytgat, J. Importance of position 8 in μ-conotoxin KIIIA for voltage-gated sodium channel selectivity. *FEBS J.* **2011**, *278*, 3408–3418. [CrossRef]

14. Khoo, K.K.; Wilson, M.J.; Smith, B.J.; Zhang, M.M.; Gulyas, J.; Yoshikami, D.; River, J.E.; Bulaj, G.; Norton, R.S. Lactam-stabilized helical analogues of the analgesic μ-conotoxin KIIIA. *J. Med. Chem.* **2011**, *54*, 7558–7566. [CrossRef] [PubMed]

15. Brady, R.M.; Zhang, M.; Gable, R.; Norton, R.S.; Baell, J.B. De novo design and synthesis of a μ-conotoxin KIIIA peptidomimetic. *Bioorg. Med. Chem. Lett.* **2013**, *23*, 4892–4895. [PubMed]

16. Stevens, M.; Peigneur, S.; Dyubankova, N.; Lescrinier, E.; Herdewijn, P.; Tytgat, J.J. Design of bioactive peptides from naturally occurring μ-conotoxin structures. *Biol. Chem.* **2012**, *287*, 31382–31392.

17. Lebbe, E.K.; Peigneur, S.; Brullot, W.; Verbiest, T.; Tytgat, J. Ala-7, His-10 and Arg-12 are crucial amino acids for activity of a synthetically engineered μ-conotoxin. *Peptides* **2014**, *53*, 300–306. [CrossRef] [PubMed]

18. Peigneur, S.; Cheneval, O.; Maiti, M.; Leipold, E.; Heinemann, S.H.; Herdewijn, P.; de Lima, M.E.; Craik, D.J.; Schroeder, C.I. Where cone snails and spiders meet: Design of small cyclic sodium-channel inhibitors. *FASEB J.* **2019**, *33*, 3693–3703.

19. Peigneur, S.; da Costa Oliveira, C.; de Sousa Fonseca, F.C.; McMahon, K.L.; Mueller, A.; Cheneval, O.; Nogueira Freitas, A.C.; Starobova, H.; Gama Duarte, I.D.; Craik, D.J.; et al. Small cyclic sodium channel inhibitors. *Biochem. Pharmacol.* **2020**, *183*, 114291. [CrossRef]

20. Schroeder, C.I.; Ekberg, J.; Nielsen, K.J.; Adams, D.; Loughnan, M.L.; Thomas, L.; Adams, D.J.; Alewood, P.F.; Lewis, R.J. Neuronally selective μ-conotoxins from Conus striatus utilize an α-helical motif to target mammalian sodium channels. *J. Biol. Chem.* **2008**, *283*, 21621–21628. [PubMed]

21. Lewis, R.J.; Schroeder, C.I.; Ekberg, J.; Nielsen, K.J.; Loughnan, M.; Thomas, L.; Adams, D.A.; Drinkwater, R.; Adams, D.J.; Alewood, P.F. Isolation and structure-activity of μ-conotoxin TIIIA, a potent inhibitor of tetrodotoxin-sensitive voltage-gated sodium channels. *Mol. Pharmacol.* **2007**, *71*, 676–685. [PubMed]

22. Dekan, Z.; Mobli, M.; Pennington, M.W.; Fung, E.; Nemeth, E.; Alewood, P.F. Total Synthesis of Human Hepcidin through Regioselective Disulfide-Bond Formation by using the Safety-Catch Cysteine Protecting Group 4,4′-Dimethylsulfinylbenzhydryl. *Angew. Chem. Int. Ed. Engl.* **2014**, *53*, 2931–2944. [PubMed]

23. Tran, H.N.T.; McMahon, K.L.; Deuis, J.R.; Vetter, I.; Schroeder, C.I. Structural and functional insights into the inhibition of human voltage-gated sodium channels by μ-conotoxin KIIIA disulfide isomers. *J. Biol. Chem.* **2022**, *298*, 101728. [PubMed]

24. Wilson, M.J.; Yoshikami, D.; Azam, L.; Gajewiak, J.; Olivera, B.M.; Bulaj, G.; Zhang, M.-M. μ-Conotoxins that differentially block sodium channels NaV1.1 through 1.8 identify those responsible for action potentials in sciatic nerve. *Proc. Natl. Acad. Sci. USA* **2011**, *108*, 10302–10307.

25. Zhang, M.M.; Wilson, M.J.; Azam, L.; Gajewiak, J.; Rivier, J.E.; Bulaj, G.; Olivera, B.M.; Yoshikami, D. Co-expression of NaVβ subunits alters the kinetics of inhibition of voltage-gated sodium channels by pore-blocking μ-conotoxins. *Br. J. Pharmacol.* **2013**, *168*, 1597–1610.

26. Tran, H.N.T.; Tran, P.; Deuis, J.R.; Agwa, A.J.; Zhang, A.H.; Vetter, I.; Schroeder, C.I. Enzymatic Ligation of a Pore Blocker Toxin and a Gating Modifier Toxin: Creating Double-Knotted Peptides with Improved Sodium Channel NaV1.7 Inhibition. *Bioconjug. Chem.* **2020**, *31*, 64–73.

27. Harvey, P.J.; Kurniawan, N.D.; Finol-Urdaneta, R.K.; McArthur, J.R.; van Lysebetten, D.; Dash, T.S.; Hill, J.M.; Adams, D.J.; Durek, T.; Craik, D.J. NMR Structure of μ-Conotoxin GIIIC: Leucine 18 Induces Local Repacking of the N-Terminus Resulting in Reduced NaV Channel Potency. *Molecules* **2018**, *23*, 2715. [CrossRef]

28. Leipold, E.; Ullrich, F.; Thiele, M.; Tietze, A.A.; Terlau, H.; Imhof, D.; Heinermann, S.H. Subtype-specific block of voltage-gated K+ channels by μ-conopeptides. *Biochem. Biophys. Res. Commun.* **2017**, *482*, 1135–1140.

29. Khoo, K.K.; Gupta, K.; Green, B.R.; Zhang, M.M.; Watkins, M.; Olivera, B.M.; Balaram, P.; Yoshikami, D.; Bulaj, G.; Norton, R.S. Distinct disulfide isomers of μ-conotoxins KIIIA and KIIIB block voltage-gated sodium channels. *Biochemistry* **2012**, *51*, 9826–9835.

30. Wishart, D.S.; Bigam, C.G.; Holm, A.; Hodges, R.S.; Sykes, B.D. 1H, 13C and 15N random coil NMR chemical shifts of the common amino acids. I. Investigations of nearest-neighbor effects. *J. Biomol. NMR* **1995**, *5*, 67–81.

31. Keizer, D.W.; West, P.J.; Lee, E.F.; Yoshikami, D.; Olivera, B.M.; Bulaj, G.; Norton, R.S. Structural basis for tetrodotoxin-resistant sodium channel binding by μ-conotoxin SmIIIA. *J. Biol. Chem.* **2003**, *278*, 46805–46813. [PubMed]

32. Khoo, K.K.; Feng, Z.P.; Smith, B.J.; Zhang, M.M.; Yoshikami, D.; Olivera, B.M.; Bulaj, G.; Norton, R.S. Structure of the analgesic μ-conotoxin KIIIA and effects on the structure and function of disulfide deletion. *Biochemistry* **2009**, *48*, 1210–1219.

33. Green, B.R.; Catlin, P.; Zhang, M.M.; Fiedler, B.; Bayudan, W.; Morrison, A.; Norton, R.S.; Smith, B.J.; Yoshikami, D.; Olivera, B.M.; et al. Conotoxins Containing Nonnatural Backbone Spacers: Cladistic-Based Design, Chemical Synthesis, and Improved Analgesic Activity. *Chem. Biol.* **2007**, *14*, 399–407. [PubMed]

34. Jacob, R.B.; McDougal, O.M. The M-superfamily of conotoxins: A review. *Cell. Mol. Life Sci.* **2010**, *67*, 17–27.

35. Paul George, A.A.; Heimer, P.; Maass, A.; Hamaekers, J.; Hofmann-Apitius, M.; Biswas, A.; Imhof, D. Insights into the folding of disulfide-rich μ-conotoxins. *ACS Omega* **2018**, *3*, 12330–12340. [PubMed]

36. Sato, K.; Ishida, Y.; Wakamatsu, K.; Kato, R.; Honda, H.; Ohizumi, Y.; Nakamura, H.; Ohya, M.; Lancelin, J.M.; Khoda, D. Active site of mu-conotoxin GIIIA, a peptide blocker of muscle sodium channels. *J. Biol. Chem.* **1991**, *266*, 16989–16991. [PubMed]

37. Pan, X.; Li, Z.; Huang, X.; Huang, G.; Gao, S.; Shen, H.; Liu, L.; Lei, J.; Yan, N. Molecular basis for pore blockade of human Na+ channel Nav1.2 by the μ-conotoxin KIIIA. *Science* **2019**, *363*, 1309–1313. [PubMed]